NASA TECHNICAL NOTE

NASA TN D-8237

NASA TN D-8237

SOME ANOMALIES OBSERVED IN WIND-TUNNEL TESTS OF A BLUNT BODY AT TRANSONIC AND SUPERSONIC SPEEDS

Joseph D. Brooks

Langley Research Center
Hampton, Va. 23665

NATIONAL AERONAUTICS AND SPACE ADMINISTRATION • WASHINGTON, D. C. • JUNE 1976

1. Report No.
NASA TN D-8237

2. Government Accession No.

3. Recipient's Catalog No.

4. Title and Subtitle
SOME ANOMALIES OBSERVED IN WIND-TUNNEL TESTS OF A BLUNT BODY AT TRANSONIC AND SUPERSONIC SPEEDS

5. Report Date
June 1976

6. Performing Organization Code

7. Author(s)
Joseph D. Brooks

8. Performing Organization Report No.
L-10784

9. Performing Organization Name and Address
NASA Langley Research Center
Hampton, Va. 23665

10. Work Unit No.
506-26-20-05

11. Contract or Grant No.

12. Sponsoring Agency Name and Address
National Aeronautics and Space Administration
Washington, D.C. 20546

13. Type of Report and Period Covered
Technical Note

14. Sponsoring Agency Code

15. Supplementary Notes

16. Abstract

An investigation of anomalies observed in wind-tunnel force tests of a blunt-body configuration (0.259- and 0.367-scale models of the proposed Pioneer Venus small probe configuration) was conducted at Mach numbers from 0.20 to 1.35 in the Langley 8-foot transonic pressure tunnel and at Mach numbers of 1.50, 1.80, and 2.16 in the Langley Unitary Plan wind tunnel. The Reynolds number, based on the maximum diameter of the model, varied from 2.25×10^6 to 2.75×10^6 in the 8-foot transonic pressure tunnel and from 1.3×10^6 to 3.3×10^6 in the Unitary Plan wind tunnel.

At a Mach number of 1.35, large variations occurred in axial-force coefficient at a given angle of attack. At transonic and low supersonic speeds, the total drag measured in the wind tunnel was much lower than that measured during earlier ballistic range tests. Accurate measurements of total drag for blunt bodies will require the use of models smaller than those tested thus far; however, it appears that accurate forebody drag results can be obtained by using relatively large models. Shock standoff distance is presented from experimental data over the Mach number range from 1.05 to 4.34. Theory accurately predicts the shock standoff distance at Mach numbers up to 1.75.

17. Key Words (Suggested by Author(s))
Blunt-body drag – wind tunnel
Transonic drag
Supersonic drag

18. Distribution Statement
Unclassified – Unlimited

Subject Category 18

19. Security Classif. (of this report)	20. Security Classif. (of this page)	21. No. of Pages	22. Price*
Unclassified	Unclassified	25	$3.25

*For sale by the National Technical Information Service, Springfield, Virginia 22161

SOME ANOMALIES OBSERVED IN WIND-TUNNEL TESTS OF A BLUNT BODY AT TRANSONIC AND SUPERSONIC SPEEDS

Joseph D. Brooks
Langley Research Center

SUMMARY

An investigation of anomalies observed in wind-tunnel force tests of a blunt-body configuration (0.259- and 0.367-scale models of the proposed Pioneer Venus small probe configuration) was conducted at Mach numbers from 0.20 to 1.35 in the Langley 8-foot transonic pressure tunnel and at Mach numbers of 1.50, 1.80, and 2.16 in the Langley Unitary Plan wind tunnel. The Reynolds number, based on the maximum diameter of the model, varied from 2.25×10^6 to 2.75×10^6 in the 8-foot transonic pressure tunnel and from 1.3×10^6 to 3.3×10^6 in the Unitary Plan wind tunnel.

At a Mach number of 1.35, large variations occurred in axial-force coefficient at a given angle of attack. At transonic and low supersonic speeds, the total drag measured in the wind tunnel was much lower than that measured during earlier ballistic range tests. Accurate measurements of total drag for blunt bodies will require the use of models smaller than those tested thus far; however, it appears that accurate forebody drag results can be obtained by using relatively large models. Shock standoff distance is presented from experimental data over the Mach number range from 1.05 to 4.34. Theory accurately predicts the shock standoff distance at Mach numbers up to 1.75.

INTRODUCTION

With the advent of the space research programs, many blunt-body configurations have been tested in the Langley 8-foot transonic pressure tunnel. These include the reentry configurations for the Mercury and Apollo projects, the Viking entry and lander configurations, and the Pioneer Venus probe.

In designing these blunt-body configurations, it is essential that the aerodynamic characteristics measured in the wind tunnel be accurate in order to assess the performance of the body shapes. The purpose of this paper is to investigate some of the anomalies which can occur in wind-tunnel investigations of blunt bodies.

During an investigation to obtain the aerodynamic characteristics of the Pioneer Venus probes in the Langley 8-foot transonic pressure tunnel, the bow shock wave did not appear to be reflected from the walls of the tunnel in the schlieren pictures at a Mach number of 1.20. Apparently, the shock reflection was hidden either in itself or in the region where the shock intersects the window of the tunnel. This indicates that the model was too large for the 8-foot transonic pressure tunnel and resulted in tunnel-wall interference effects. Furthermore, the drag data from this investigation did not correlate with the drag data obtained from ballistic range tests at corresponding supersonic Mach numbers. (See ref. 1.)

The blockage of the Pioneer Venus probes used in the present investigation was about the same, 27.94 cm (11.00 in.) in diameter, as that used in previous blunt-body investigations in the 8-foot transonic pressure tunnel. Because of the difficulty in observing the shock reflection in the schlieren pictures at a Mach number of 1.20 and the discrepancies in the drag data, the investigation was expanded to include a smaller model with one-half the blockage, 19.76 cm (7.78 in.) in diameter, of the original configuration.

The investigation was conducted at Mach numbers from 0.20 to 1.35 in the Langley 8-foot transonic pressure tunnel and at Mach numbers of 1.50, 1.80, and 2.16 in the Langley Unitary Plan wind tunnel. The Reynolds number, based on the maximum diameter of the model, varied from 2.25×10^6 to 2.75×10^6 in the 8-foot transonic pressure tunnel and from 1.3×10^6 to 3.3×10^6 in the Unitary Plan wind tunnel.

SYMBOLS

The aerodynamic data presented herein are referred to the body-axis system with the origin located at the center of gravity of the configuration as shown in figure 1. Values are given both in SI Units and U.S. Customary Units. The measurements and calculations were made in U.S. Customary Units.

$C_{A,corr}$ axial-force coefficient corrected for base pressure, $\frac{\text{Total axial force}}{qS} + \frac{p_b - p}{q}$

$C_{A,uncorr}$ total axial-force coefficient, $\frac{\text{Total axial force}}{qS}$

$C_{D,fore}$ forebody drag coefficient at $\alpha = 0^\circ$ $\left(\text{the same as } C_{A,corr}\right)$, $\frac{\text{Total drag force}}{qS} + \frac{p_b - p}{q}$

$C_{D,total}$ total drag coefficient at $\alpha = 0^\circ$ $\left(\text{the same as } C_{A,uncorr}\right)$, $\frac{\text{Total drag force}}{qS}$

C_m pitching-moment coefficient, $\frac{\text{Pitching moment}}{qSd}$

C_N normal-force coefficient, $\frac{\text{Normal force}}{qS}$

C_p pressure coefficient, $\frac{p_l - p}{q}$

$C_{p,b}$ base pressure coefficient, $\frac{p_b - p}{q}$

d maximum body diameter, 19.76 cm (7.78 in.) for small body and 27.94 cm (11.00 in.) for larger body

M free-stream Mach number

p free-stream static pressure

p_b average static pressure at model base

p_l local static pressure

q free-stream dynamic pressure

R Reynolds number based on d

r radius of curvature

r_{body} maximum body radius, 9.88 cm (3.89 in.) for small body and 13.97 cm (5.5 in.) for large body

S base area, $\pi d^2/4$, 306.5 cm^2 (47.5 in^2) for small body and 613 cm^2 (95.0 in^2) for large body

α angle of attack, deg

Δ shock standoff distance, measured from schlieren photographs, cm (in.)

ϵ cone half-angle, deg

APPARATUS AND TESTS

Tunnel

The investigation was conducted in the Langley 8-foot transonic pressure tunnel and in the low Mach number test section of the Langley Unitary Plan wind tunnel. The 8-foot transonic pressure tunnel has a slotted test section approximately 2.17 m (85.5 in.) square that is capable of a Mach number range from 0.20 to 1.35. The Unitary Plan wind tunnel has a test section approximately 1.22 m (48.0 in.) square. The nozzle leading to the test section of the Unitary Plan wind tunnel has an asymmetric sliding block which permits a continuous variation in test-section Mach number from 1.5 to 2.9. Both wind tunnels are continuous-flow, variable-pressure tunnels, and the air is dried sufficiently during testing to avoid condensation effects.

Models

The models used in this investigation (fig. 1) are scale models of the proposed Pioneer Venus small probe configuration. The models have a conically shaped forebody with a 90° included angle and a blunt spherical nose. The small model ($d = 19.76$ cm (7.78 in.)) is 0.259 scale and the larger model ($d = 27.94$ cm (11.00 in.)) is 0.367 scale of the Pioneer Venus small probe. The small model, which was used for the expanded portion of the investigation, was selected to have one-half the frontal area of the larger model. For some tests, instrument housing and sensors were mounted on the base of the model. These are shown in the photographs of the larger model in figure 2. The models were constructed of aluminum and were sting mounted in the tunnels. In order to have the same sting interference effects for both models in the 8-foot transonic pressure tunnel, the ratio of the maximum body diameter to the length of the untapered cylindrical sting section following the model base was 0.68. This ratio was 0.30 for the Unitary Plan wind tunnel. The ratio of the cross-sectional area of the sting to the model base area is small, 0.016 for the large model and 0.031 for the small model; therefore, the sting area effect should be almost negligible according to reference 2.

Instrumentation

The aerodynamic forces and moments were measured with a six-component, electrical, internal strain-gage balance, with the pitching moment referred to the center-of-gravity location shown in figure 1.

The model chamber pressure was measured inside the model cavity, and the base pressure was measured approximately 1.0 cm (0.4 in.) above and below the sting with differential-pressure transducers.

Tests

The large model was tested in the 8-foot transonic pressure tunnel at Mach numbers of 0.50, 0.80, 0.95, and 1.20 without the instrument housings and at Mach numbers of 0.20, 1.10, and 1.35 with the instrument housings mounted on the base of the model, as shown in the photograph of figure 2.

The small model was tested without the instrument housings in the 8-foot transonic pressure tunnel at Mach numbers of 0.95, 1.20, and 1.35 and in the Unitary Plan wind tunnel at Mach numbers of 1.50, 1.80, and 2.16. All tests were conducted over an angle-of-attack range from about -3.5° to 20°. The total temperature was held constant at approximately 322 K (120° F) in the 8-foot transonic pressure tunnel and 339 K (150° F) in the Unitary Plan wind tunnel. The stagnation pressure was varied in the tunnels to obtain the desired Reynolds numbers. The variation of Reynolds number with Mach number is shown in figure 3. Reynolds number is based on the maximum model diameter.

Corrections

Angles of attack have been corrected for the deflection of the balance and sting support under aerodynamic load and for tunnel flow angularity.

The axial-force measurements are presented both uncorrected and corrected to a condition of free-stream static pressure on the base of the model. An average base pressure was obtained by averaging the chamber pressure and the two base-pressure measurements. The average base pressure was applied to the total base area. The chamber pressure and the base pressure were approximately the same.

Accuracy

The estimated accuracies of the measurements excluding sting interference effects, blockage, or shock reflection effects are estimated to be within the following limits:

Axial-force coefficient	±0.02
Normal-force coefficient	±0.004
Pitching-moment coefficient	±0.001
Pressure coefficient	±0.02
Mach number	±0.01
Angle of attack	$\pm 0.10^{\circ}$

PRESENTATION OF RESULTS

The results of this investigation are presented in the following figures:

DISCUSSION

Force Data

The basic aerodynamic data for this investigation, presented in figures 5 to 8, indicate that the models are statically stable; however, at a Mach number of 1.10 (fig. 5) there is a nonlinear variation of C_N with α in the low angle-of-attack range. Thus, a small region of instability is noted between $\alpha = -1^{\circ}$ and $\alpha = 1^{\circ}$. No effect of Reynolds number was noted in comparing the data at the high and low Reynolds numbers at a Mach number of 1.50. A large difference in axial-force coefficient between the large and small models can be seen in figure 7 at the higher angles of attack at $M = 1.35$. However, the large model had the instrument housings on the base of the model, as shown in figure 2, which may have an effect on the axial-force anomaly. When the axial-force coefficient is corrected for base pressure (to a condition of free-stream static pressure on the base of the model), shown in figure 8, the large difference in drag is practically eliminated.

A repeat run for the small model was made at a Mach number of 1.35 to determine whether the anomaly in axial force would persist. The aerodynamic data, seen in figure 9, indicate that an unstable flow phenomenon must occur in the wake of the body, since the uncorrected axial-force coefficient is different for each run and then converges when the axial force is corrected for base pressure. The instrument housings on the large model had no apparent effect on this anomaly. The reason for this anomaly in axial force is unknown, but it may be attributed to either an unstable separation around the shoulder of the model or, possibly, sting interference effects combined with boundary-reflected disturbances that cause large variations in base pressure with small changes in tunnel conditions.

Interference Effects

During investigations in transonic and supersonic wind tunnels, it is imperative that the bow shock reflected from the wall of the tunnel not impinge on the model or that it not be reflected in proximity to the base of the model. (See ref. 3.)

During the investigation of the larger model, the reflected bow shock did not appear in the schlieren photographs at a Mach number of 1.20. This indicated that the shock reflection was hidden either in itself or in the region where the shock intersects the window of the tunnel. Because of the size of the model (d = 27.94 cm (11.00 in.)) and the blunt shape of the body, the shock standoff distance is quite large (approximately 0.7d at M = 1.20, fig. 11(a)), so that the reflected bow shock may be impinging on the model and causing large wind-tunnel interference effects. Furthermore, this anomaly is illustrated in figure 10(a) from a comparison of the drag data from this test with that obtained from the ballistic range test (ref. 1). Note the unsatisfactory correlation which exists at Mach numbers of 1.20 and 1.35 for the large model.

Because of the possible interference effect due to shock reflection, a smaller model with one-half the blockage of the larger model (that is, a ratio of cross-sectional area of the model to cross-sectional area of the tunnel of 0.656 percent instead of 1.31 percent) was tested at transonic and supersonic Mach numbers. A comparison of the data for the small model with that from the ballistic range tests (fig. 10(a)) also indicates a reduction in total drag for the wind-tunnel data at Mach numbers of 1.20, 1.35, and 1.50. At Mach numbers above 1.50 and below 1.10, the wind-tunnel data compare favorably with data from the ballistic range investigations. These data definitely support the supposition that this is an interference effect due to boundary-reflected disturbances. Even using a smaller model that moved the reflected shock farther downstream did not eliminate the anomaly.

In order to gain further insight into the total drag anomalies, schlieren photographs of the small model were taken at Mach numbers of 1.20, 1.35, 1.50, and 1.80 and are presented in figure 11. At $M = 1.20$ the bow shock wave is far forward of the nose of the model; however, the line where the shock intersects the window (sidewall) of the tunnel is behind the base of the model indicating that the wall reflected shock would be at least 2 model diameters behind the base of the small model. At Mach numbers of 1.50 and 1.80 the reflected bow shock can be seen and is well behind the base of the model (fig. 11(b)).

Forebody drag data are shown in figure 10(b) for both the small and the large models at $\alpha = 0^{\circ}$. Removing the base drag results in a smooth variation in forebody drag with Mach number. The forebody drag data from this investigation compare very closely with the forebody drag data interpolated from the experimental data in reference 4. The total drag is not presented in reference 4, since the total drag data were not considered accurate because of sting interference effects on base pressures. It should be noted that the blockage of the models used in reference 4 was 3.61 percent, which is almost 3 times the blockage of the large model tested in the Langley 8-foot transonic pressure tunnel (1.31 percent).

In figure 12, the bow-shock formation is shown in the 8-foot transonic pressure tunnel at $M = 1.20$ in conjunction with the pressure distribution along the tunnel wall. The pressure distribution appears as an N-wave, or sonic boom signature, distorted by the wall boundary layer and shock reflections. It appears that the positive pressure of the wall-reflected bow shock is focused in the low-energy wake of the body and is able to propagate its effect forward, so that it increases the base pressure of the model and reduces the total drag. In the schlieren photographs of figure 11(b), at $M = 1.5$ the wake continually expands and is notably larger than the model diameter in the region where the shock reflection intersects the wake. At $M = 1.80$, however, the wake contracts downstream, so that the shock reflection intersects the wake downstream of the wake recovery shock.

The limited nature of the present tests does not provide an explanation of the total drag variations noted. However, the results do strongly suggest that wind-tunnel measurements of the total drag of blunt bodies at transonic and low supersonic speeds is greatly influenced by the character of the wake in relation to the reflected bow wave.

As a matter of interest, the uncorrected drag for the small model at higher angles of attack is approaching the drag level that was measured on the ballistic range, as shown by the tick mark on the right of $C_{A,uncorr}$ in figure 9. Therefore, the small model must be approaching the size needed to obtain interference-free total drag data at this Mach number.

The variation of the total drag coefficient with Mach number for several blunt-body configurations is shown in figure 13. These include the Apollo spacecraft (ref. 5), the Viking entry vehicle (ref. 6), and the Pioneer Venus probes of this investigation.

Comparison of these results with those of the present investigation indicates the likely presence of similar wall interference effects.

Shock Standoff Distance

The variation of the shock standoff distance ratio Δ/r_{body} with Mach number in figure 14 shows a very good correlation for data from this investigation with data from the ballistic range (ref. 1). At Mach numbers from 1.02 to 1.62, the shock standoff distance can be predicted by using the theoretical results of reference 7. At Mach numbers from 1.20 to 4.5, the shock standoff distance can be predicted by using the theoretical results of reference 8; however, at Mach numbers above 1.75, there is a large decrease in the accuracy of the theoretically predicted values. For the theoretical results presented, a spherical body with the same radius as the maximum body radius is assumed. This, apparently, is not a good assumption at the higher Mach numbers.

CONCLUDING REMARKS

An investigation of anomalies observed in wind-tunnel tests of a blunt body at transonic and supersonic speeds was conducted at Mach numbers from 0.20 to 2.16. At a Mach number of 1.35, an unstable flow phenomenon in the wake of the bodies resulted in large variations in the total axial-force coefficient at a given angle of attack. At transonic and low supersonic speeds the total drag measured in the wind tunnel was much lower than that measured during earlier ballistic range tests. Apparently, these anomalies are due to boundary-reflected disturbances that interact with the model wake and cause large variations in base pressure.

On the basis of ballistic range results, accurate measurements of total drag for these blunt bodies require the use of models smaller than those tested thus far. Further tests will be required, however, to define the appropriate size accurately. From comparisons with other results, it appears that accurate forebody drag results can be obtained at transonic speeds by using relatively large models.

The ratio of shock standoff distance to the body radius is presented from experimental data over the Mach number range from 1.05 to 4.34. Theory accurately predicts the shock standoff distance at Mach numbers up to 1.75.

Langley Research Center
National Aeronautics and Space Administration
Hampton, Va. 23665
April 15, 1976

REFERENCES

1. Weinberg, S. A.; and Pouder, J. M.: Final Data Report – Phase I Pioneer Venus Pressurized Ballistic Range Tests. 9154-TDM-74-022, Adv. Aerothermodyn. Exp. Eng., General Electric Co., Nov. 21, 1974.

2. Cahn, Maurice S.: An Experimental Investigation of Sting-Support Effects on Drag and a Comparison With Jet Effects at Transonic Speeds. NACA Rep. 1353, 1958. (Supersedes NACA RM L56F18a.)

3. Bielat, Ralph P.; Luoma, Arvo A.; and Daugherty, James C.: Drag Measurements From Different Wind Tunnels. NASA TM X-1271, 1966.

4. Owens, Robert V.: Aerodynamic Characteristics of Spherically Blunted Cones at Mach Numbers From 0.5 to 5.0. NASA TN D-3088, 1965.

5. Pearson, Albin O.: Wind-Tunnel Investigation of the Longitudinal Aerodynamic Characteristics of Models of Reentry and Atmospheric-Abort Configurations of a Proposed Apollo Spacecraft at Mach Numbers From 0.30 to 1.20. NASA TM X-604, 1961.

6. McGhee, Robert J.; Siemers, Paul M., III; and Pelc, Richard E.: Transonic Aerodynamic Characteristics of the Viking Entry and Lander Configurations. NASA TM X-2354, 1971.

7. Jones, D. J.; and South, J. C., Jr.: A Numerical Determination of the Bow Shock Wave in Transonic Axisymmetric Flow About Blunt Bodies. Aeronaut. Rep. LR-586 (NRC No. 14765), Nat. Res. Counc. of Canada, May 1975. (Available as NASA TM X-72448.)

8. Van Dyke, Milton D.; and Gordon, Helen D.: Supersonic Flow Past a Family of Blunt Axisymmetric Bodies. NASA TR R-1, 1959.

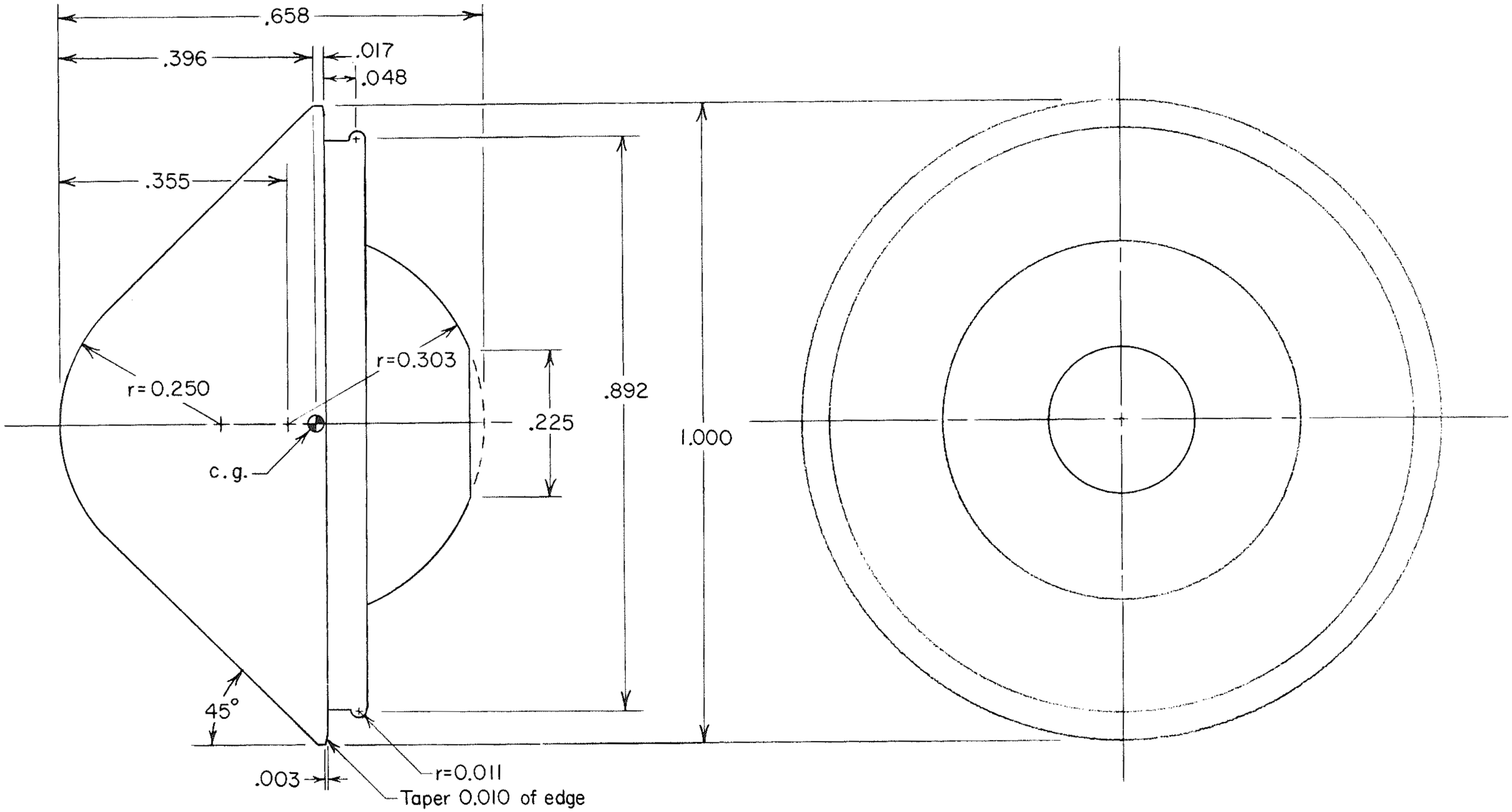

Figure 1.- Drawing of blunt-body configuration. All dimensions have been nondimensionalized by the maximum body diameter d. (d = 19.76 cm (7.78 in.) for small body and d = 27.94 cm (11.00 in.) for large body.)

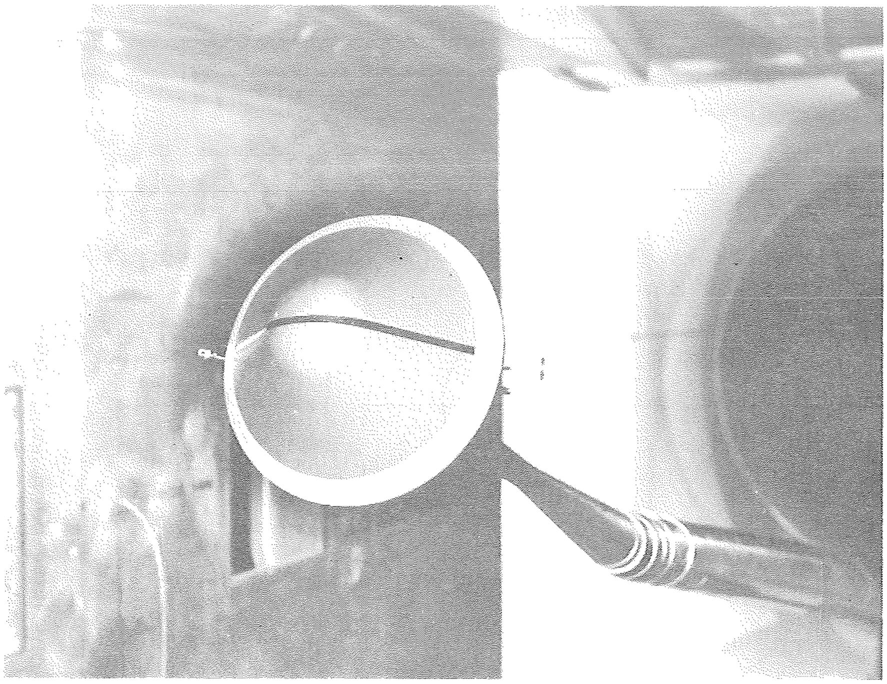

Front view L-75-2608

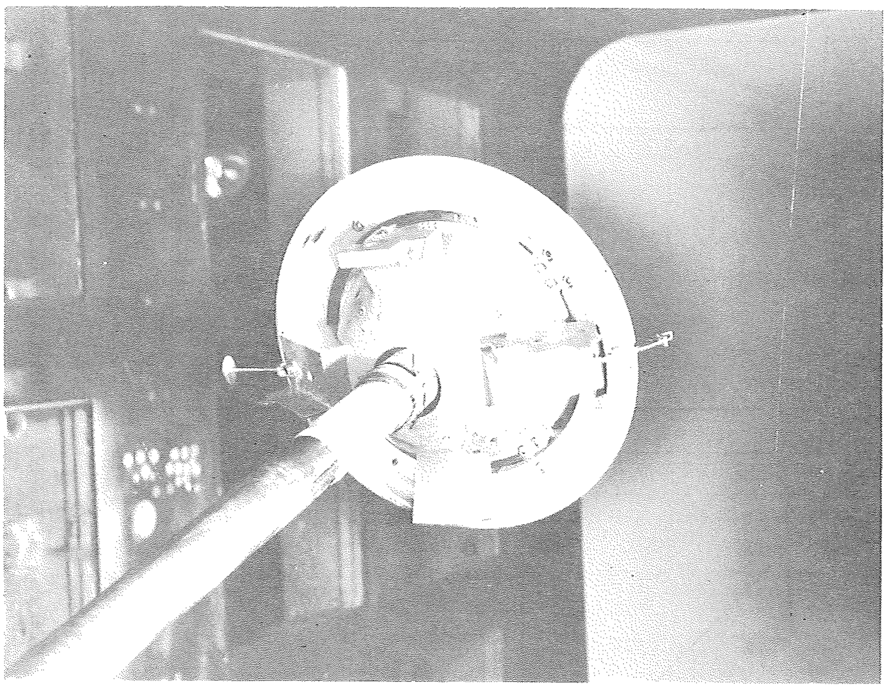

Rear view L-75-2606

Figure 2.- Large model with instrument housings on base of model in Langley 8-foot transonic pressure tunnel.

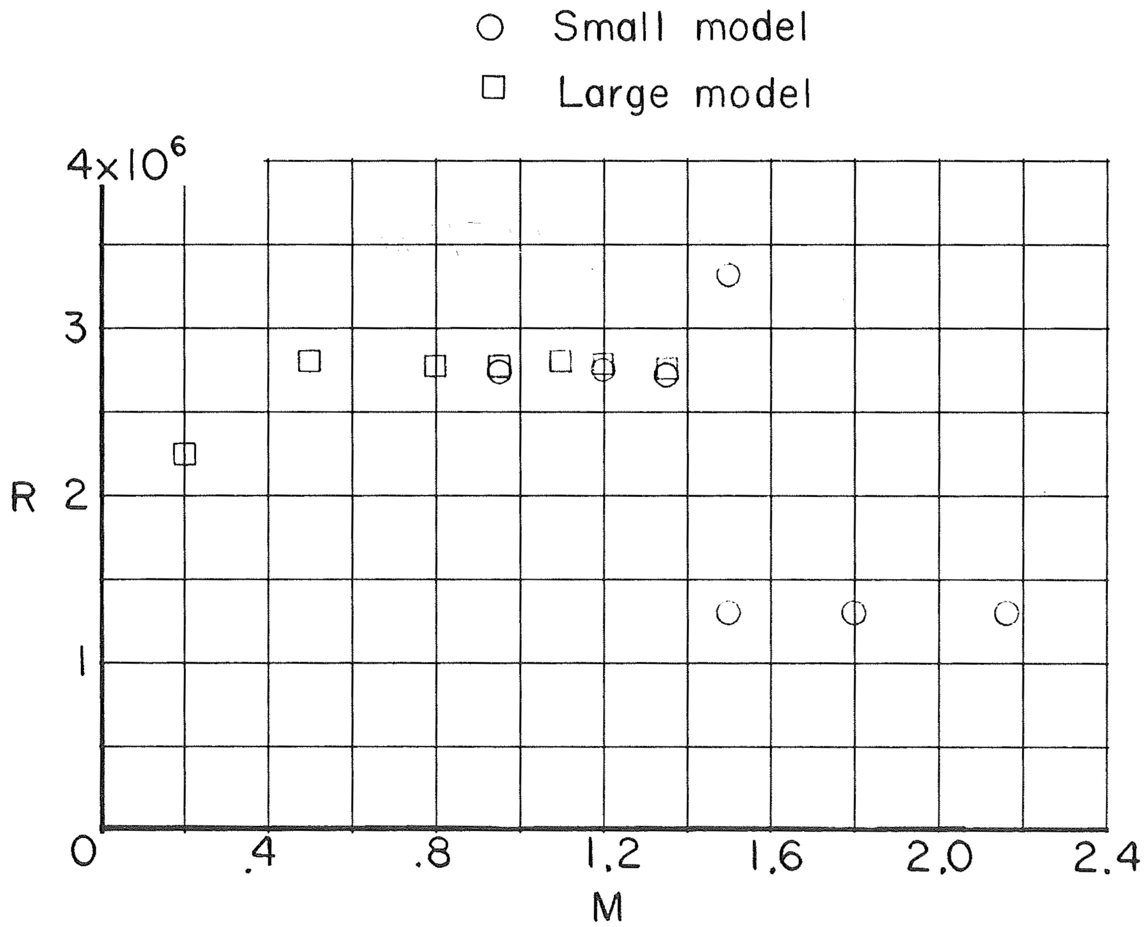

Figure 3.- Variation of Reynolds number with Mach number. (Reynolds number is based on model diameter.)

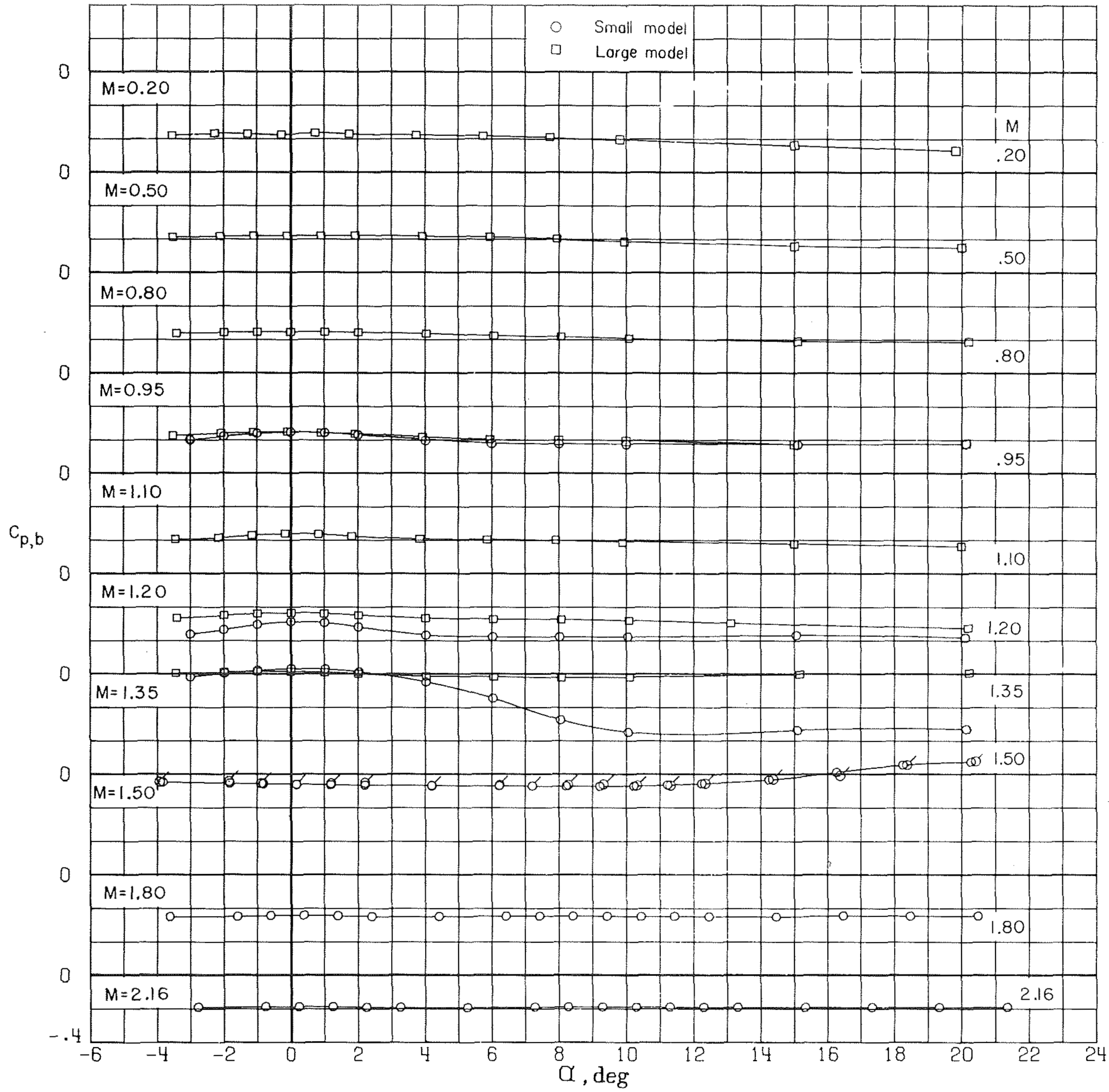

Figure 4.- Variation of average base-pressure coefficient with angle of attack. Flagged symbols indicate high Reynolds number data.

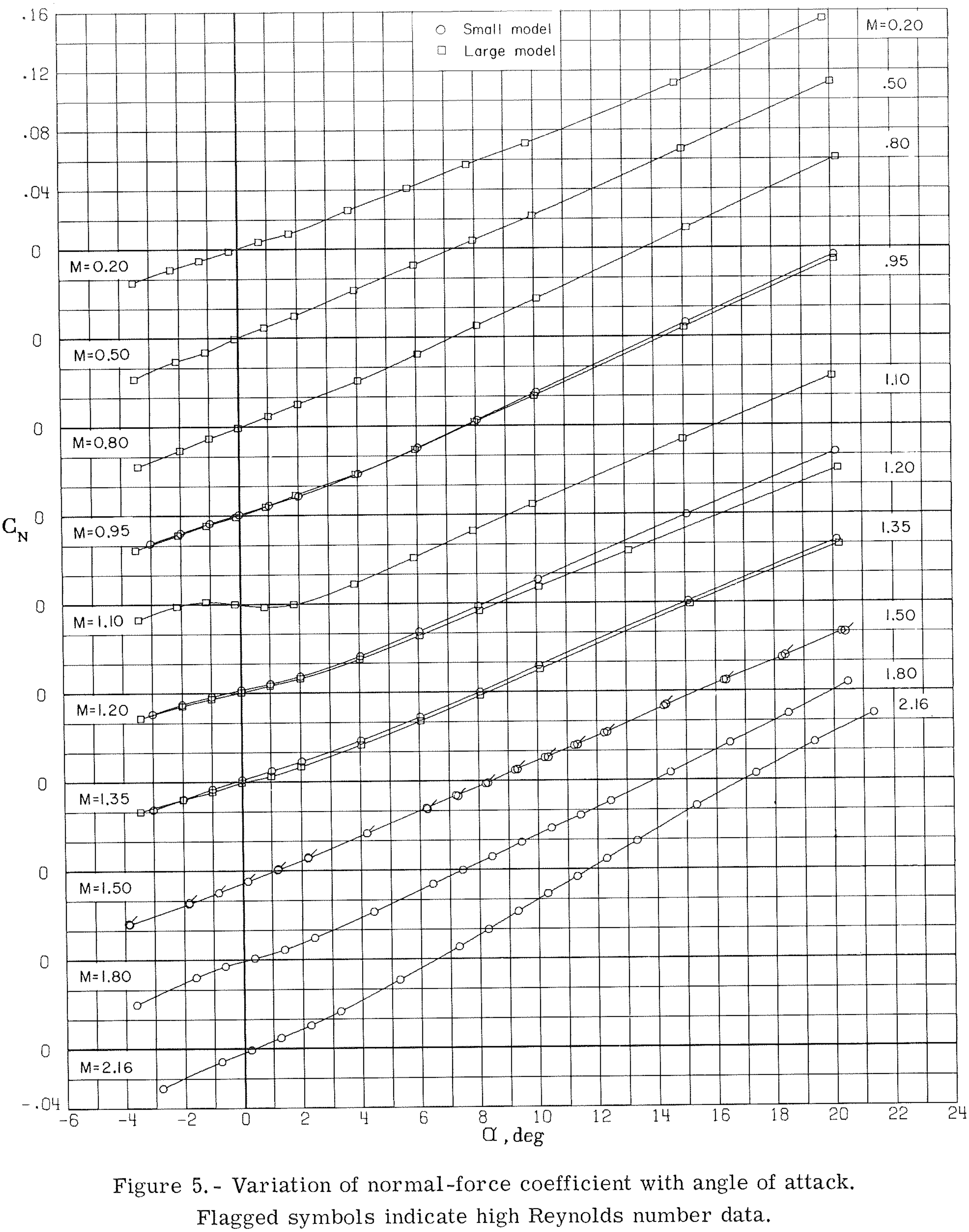

Figure 5.- Variation of normal-force coefficient with angle of attack. Flagged symbols indicate high Reynolds number data.

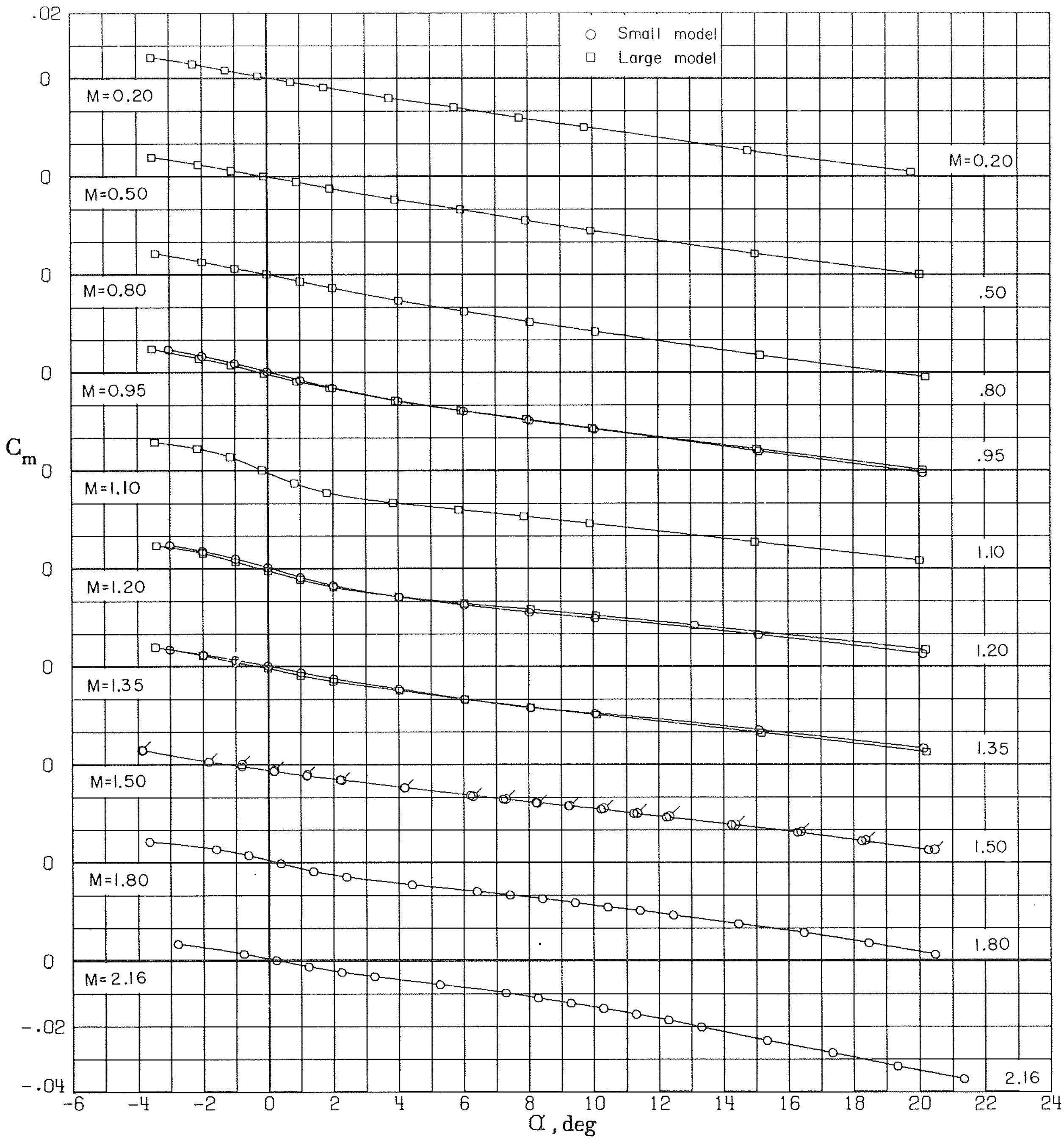

Figure 6.- Variation of pitching-moment coefficient with angle of attack. Flagged symbols indicate high Reynolds number data.

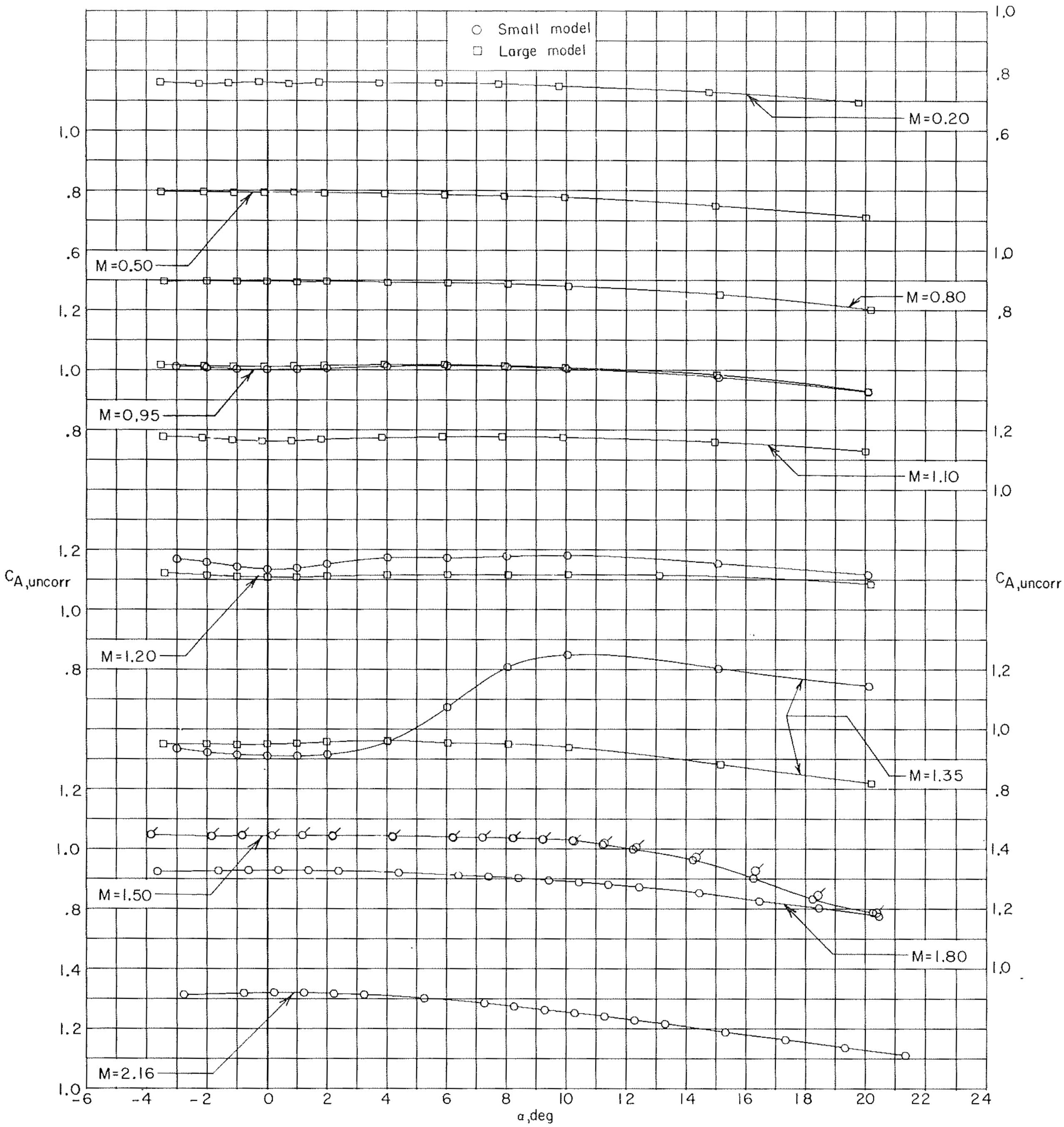

Figure 7.- Variation of axial-force coefficient, uncorrected for base pressure, with angle of attack. Flagged symbols indicate high Reynolds number data.

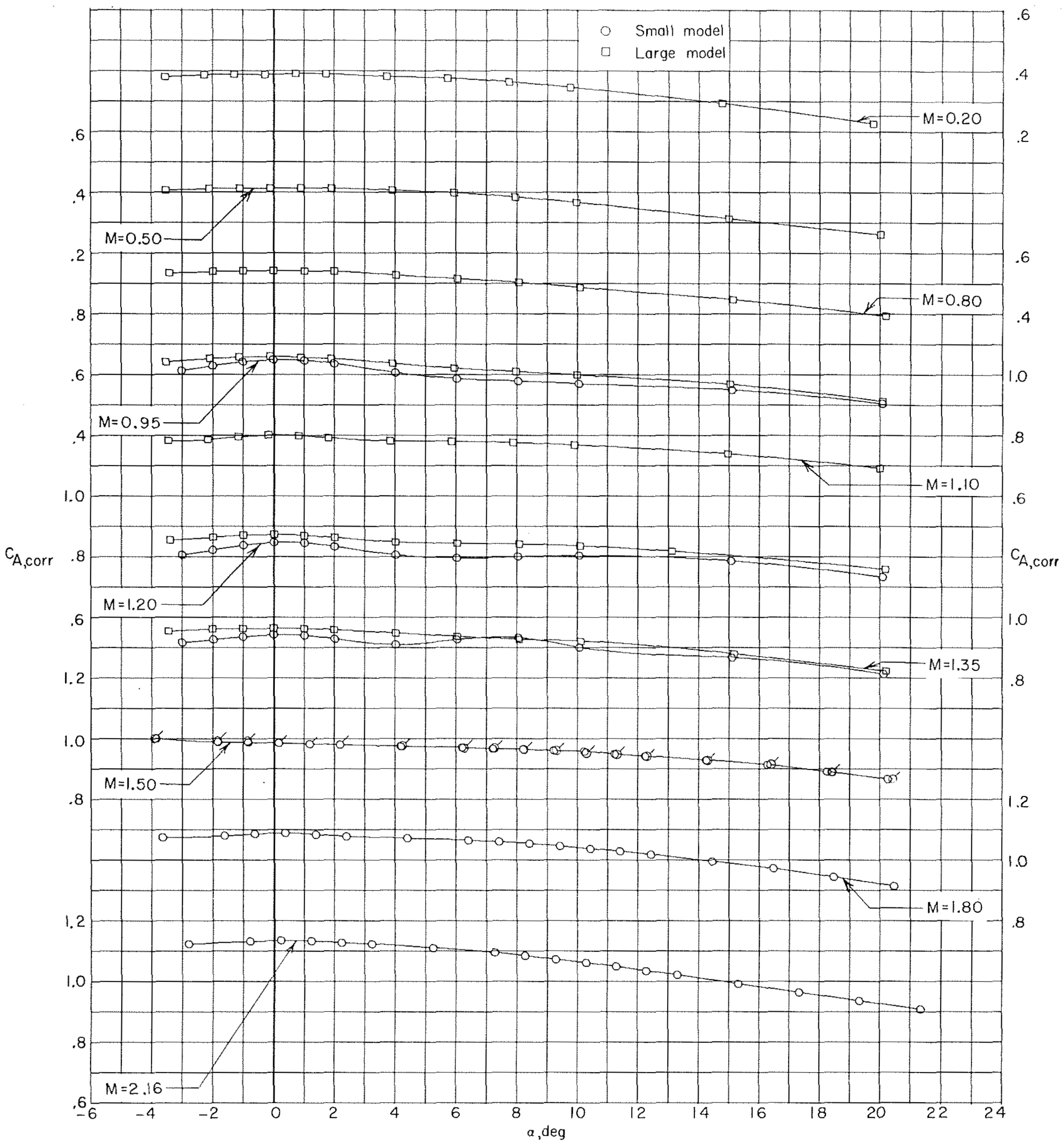

Figure 8.- Variation of axial-force coefficient, corrected for base pressure, with angle of attack. Flagged symbols indicate high Reynolds number data.

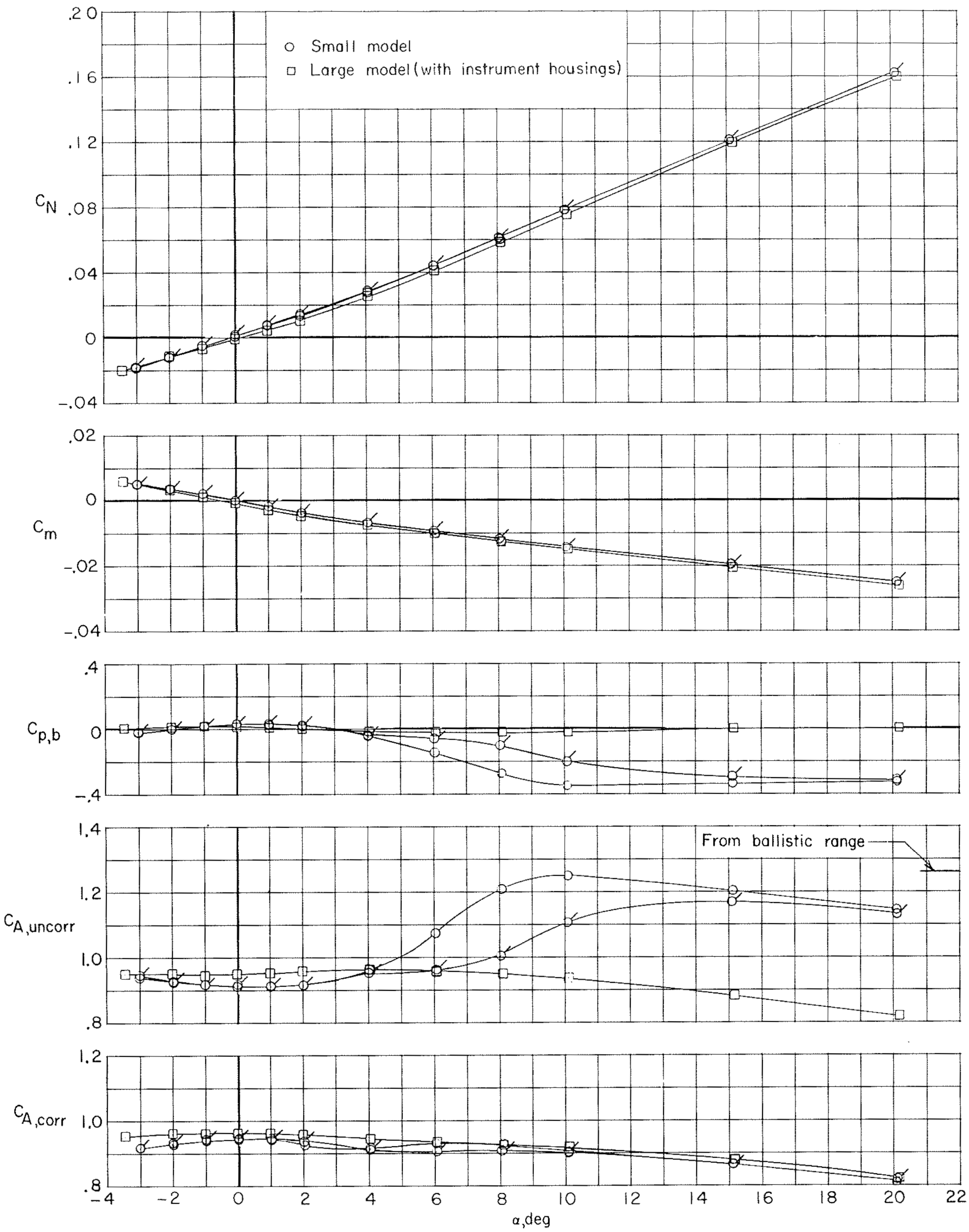

Figure 9.- Variation of aerodynamic characteristics of blunt-body configuration with angle of attack at M = 1.35. Flagged symbols indicate repeat run.

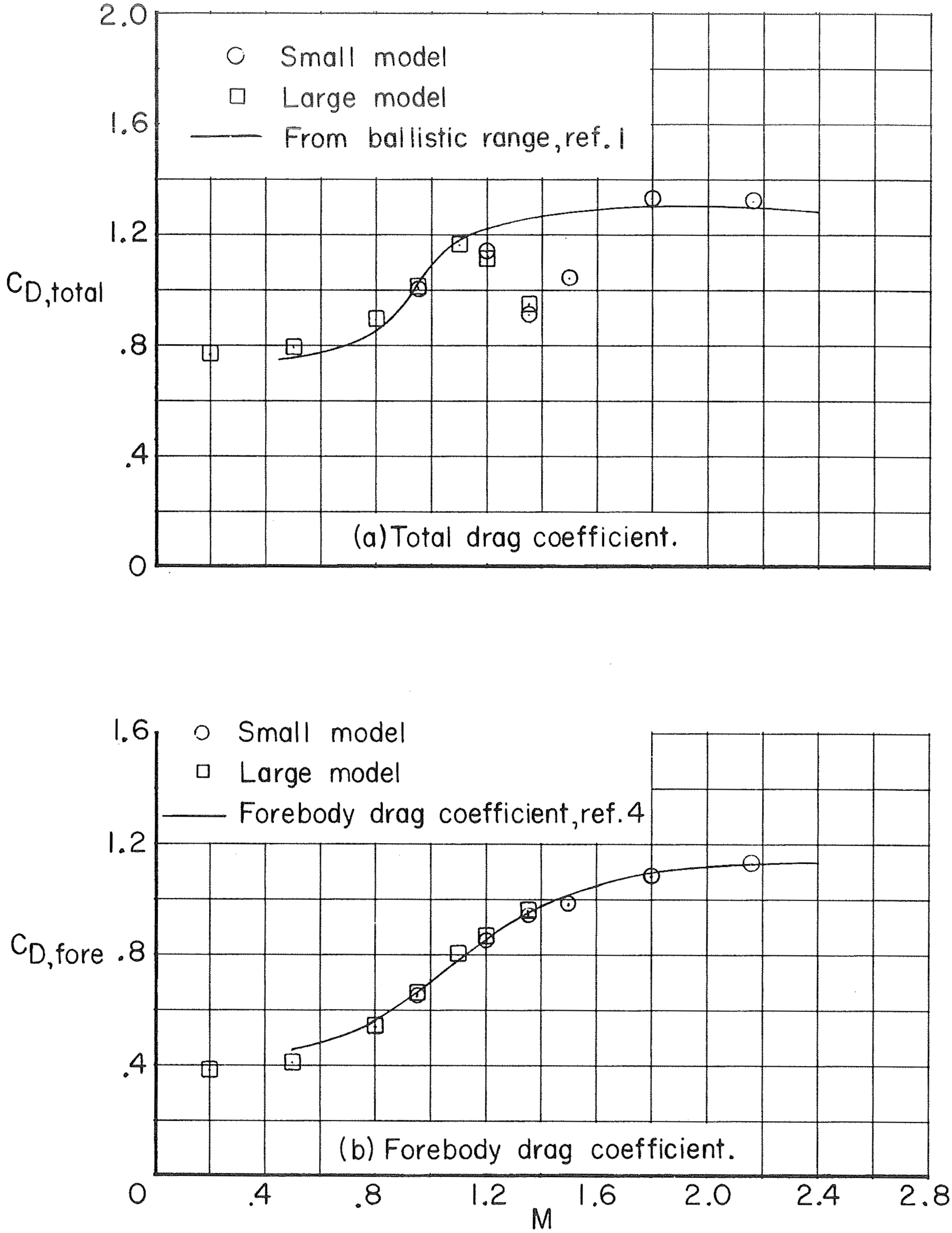

Figure 10.- Variation of total drag coefficient and forebody drag coefficient with Mach number at $\alpha = 0^{\circ}$.

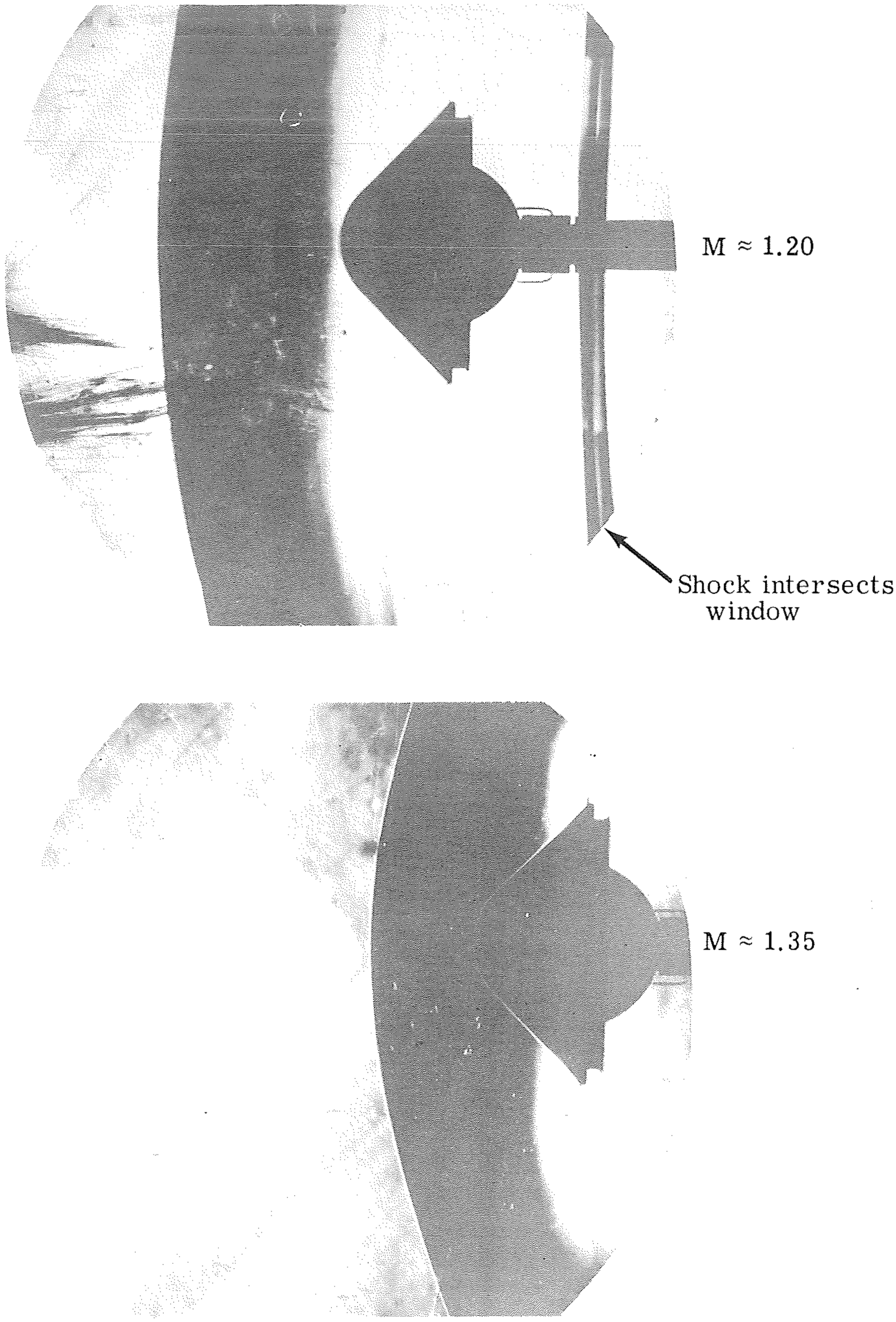

L-76-188

(a) In Langley 8-foot transonic pressure tunnel.

Figure 11.- Schlieren photographs of small body at $\alpha \approx 0^{\circ}$.

M ≈ 1.50

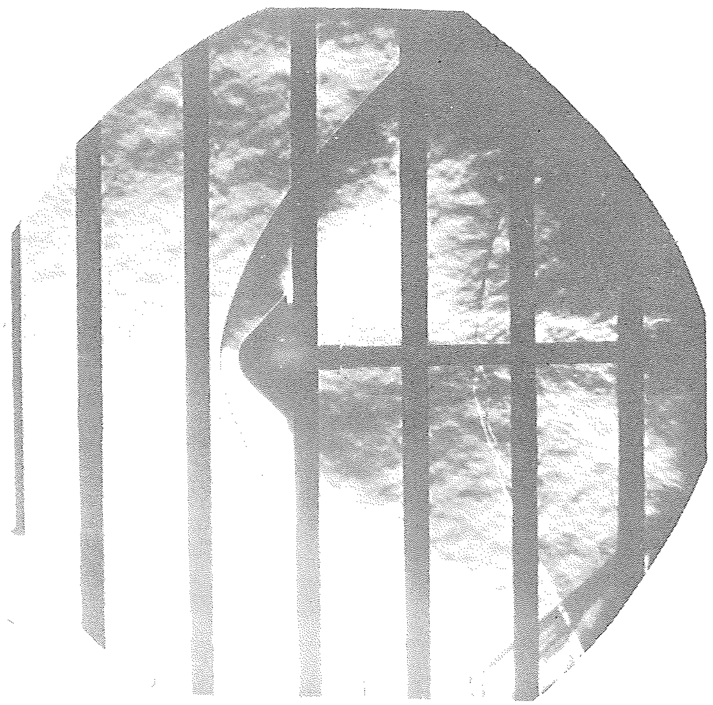

M ≈ 1.80

L-76-189

(b) In Langley Unitary Plan wind tunnel.

Figure 11.- Concluded.

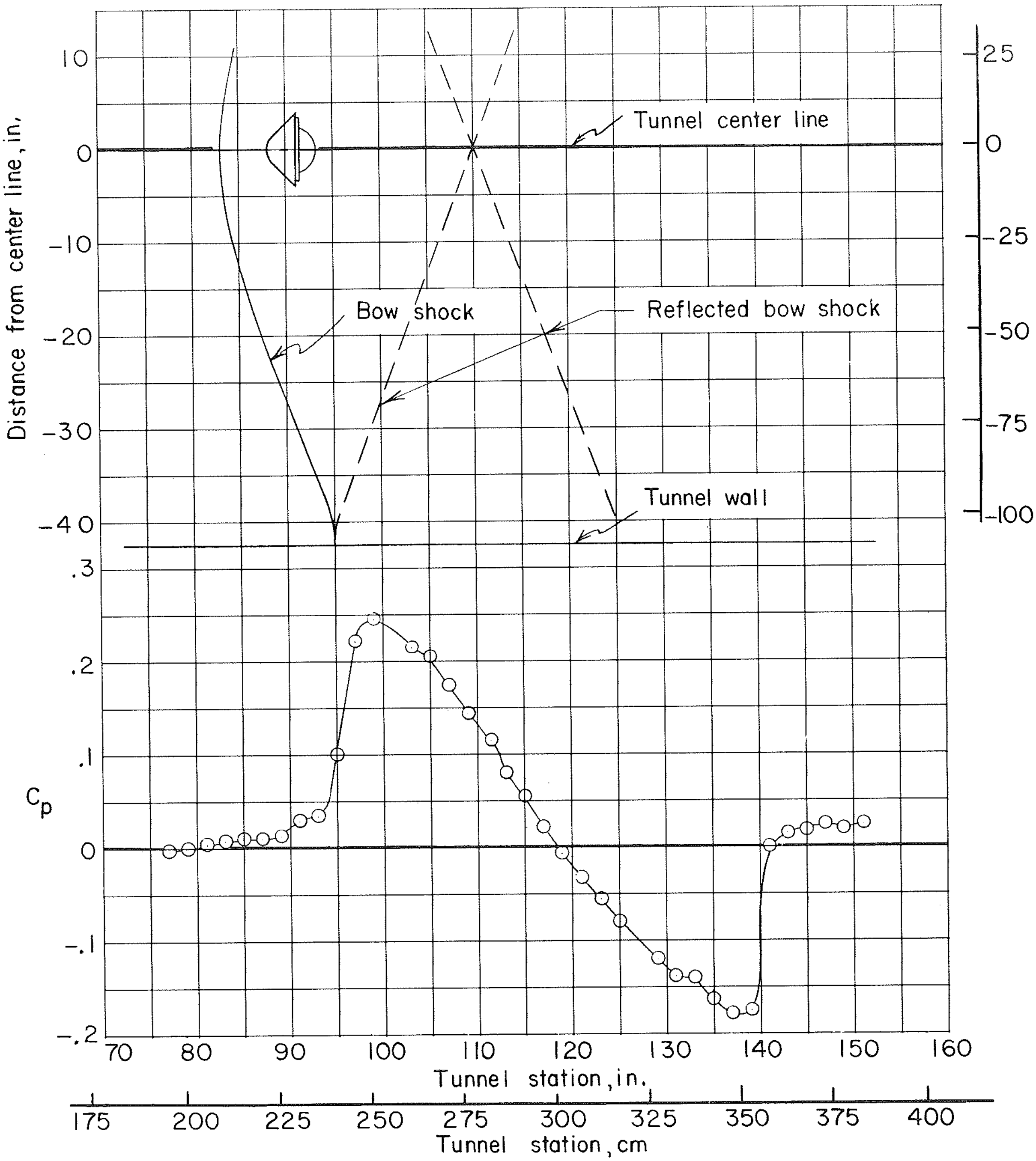

Figure 12.- Sketch of bow-shock formation for small model in conjunction with pressure distribution along wall of the Langley 8-foot transonic pressure tunnel at M = 1.20.

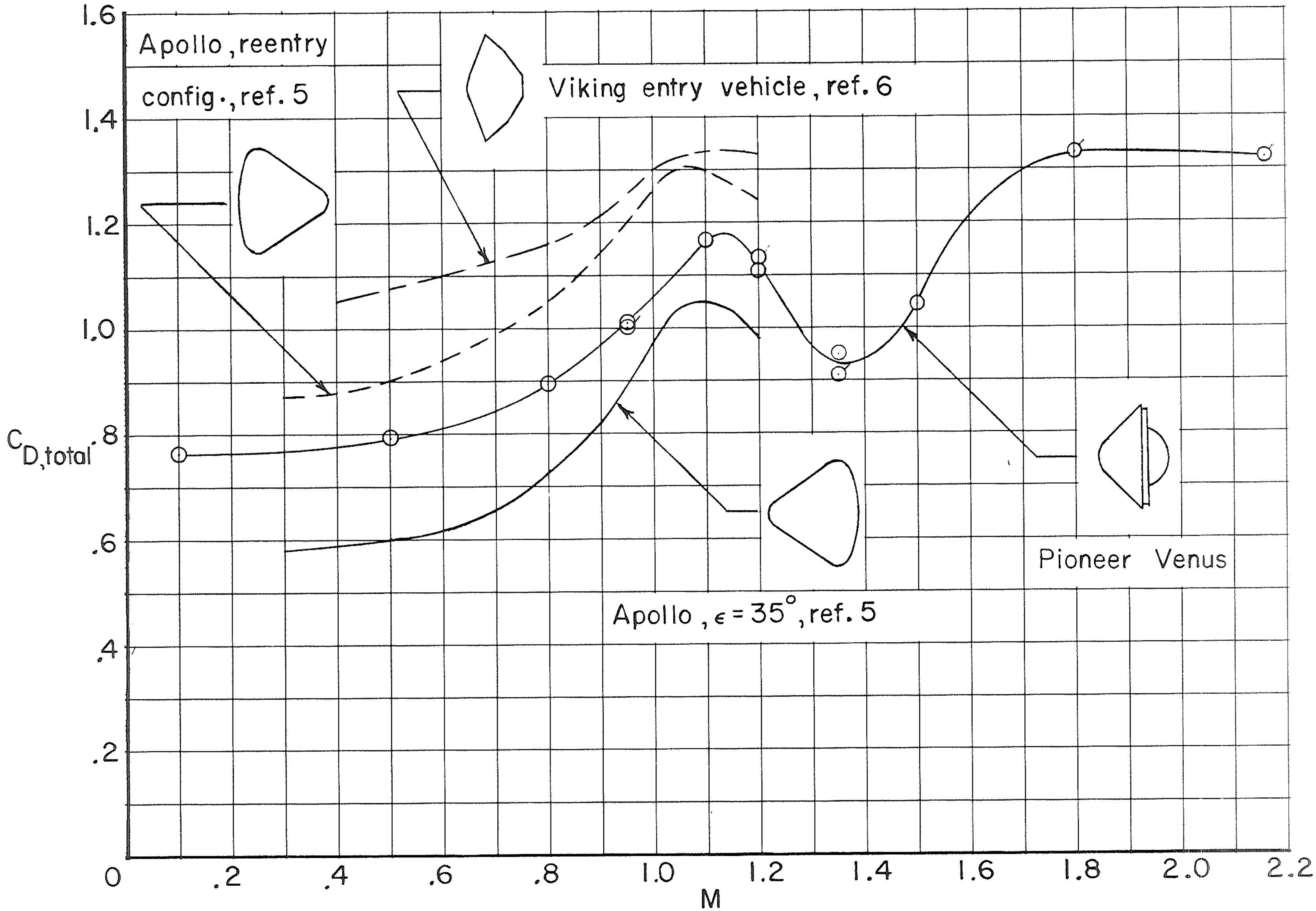

Figure 13.- Variation of total drag coefficient with Mach number for various blunt-body configurations at $\alpha = 0^{o}$. Flagged symbols indicate small model.

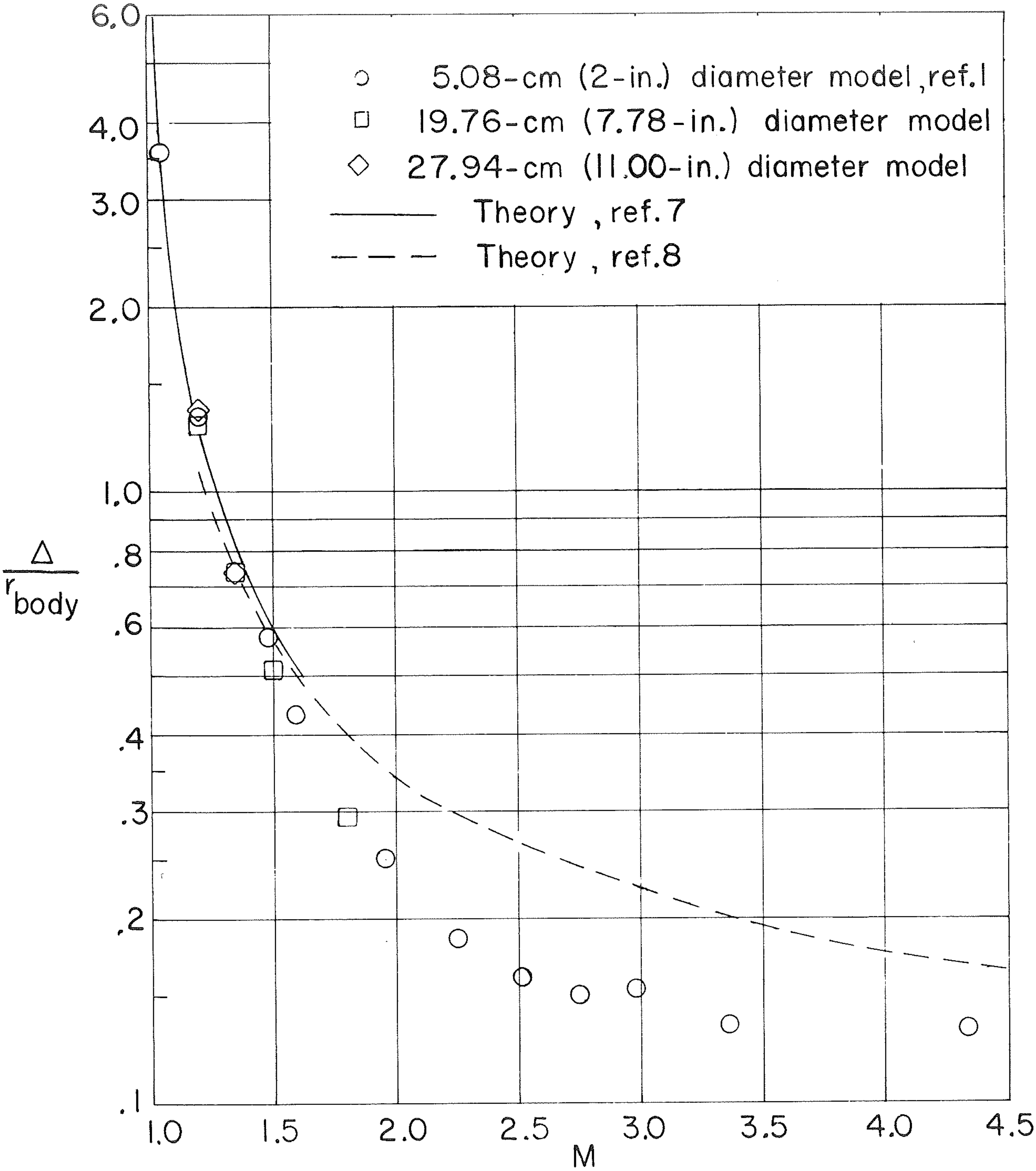

Figure 14.- Variation of shock standoff distance with Mach number.

"The aeronautical and space activities of the United States shall be conducted so as to contribute . . . to the expansion of human knowledge of phenomena in the atmosphere and space. The Administration shall provide for the widest practicable and appropriate dissemination of information concerning its activities and the results thereof."

—NATIONAL AERONAUTICS AND SPACE ACT OF 1958

NASA SCIENTIFIC AND TECHNICAL PUBLICATIONS

TECHNICAL REPORTS: Scientific and technical information considered important, complete, and a lasting contribution to existing knowledge.

TECHNICAL NOTES: Information less broad in scope but nevertheless of importance as a contribution to existing knowledge.

TECHNICAL MEMORANDUMS: Information receiving limited distribution because of preliminary data, security classification, or other reasons. Also includes conference proceedings with either limited or unlimited distribution.

CONTRACTOR REPORTS: Scientific and technical information generated under a NASA contract or grant and considered an important contribution to existing knowledge.

TECHNICAL TRANSLATIONS: Information published in a foreign language considered to merit NASA distribution in English.

SPECIAL PUBLICATIONS: Information derived from or of value to NASA activities. Publications include final reports of major projects, monographs, data compilations, handbooks, sourcebooks, and special bibliographies.

TECHNOLOGY UTILIZATION PUBLICATIONS: Information on technology used by NASA that may be of particular interest in commercial and other non-aerospace applications. Publications include Tech Briefs, Technology Utilization Reports and Technology Surveys.

Details on the availability of these publications may be obtained from:

SCIENTIFIC AND TECHNICAL INFORMATION OFFICE

NATIONAL AERONAUTICS AND SPACE ADMINISTRATION

Washington, D.C. 20546